J. Quant. Spectrosc. Radiat. Transfer. Vol. 9, pp. 775–798. Pergamon Press 1969. Printed in Great Britain

LINE BY LINE CALCULATION OF SPECTRA FROM DIATOMIC MOLECULES AND ATOMS ASSUMING A VOIGT LINE PROFILE

J. O. ARNOLD, E. E. WHITING and G. C. LYLE

Ames Research Center, NASA, Moffett Field, California 94035

(*Received* 27 *September* 1968)

Abstract A computer program is described that predicts the spectra resulting from electronic transitions of diatomic molecules and atoms. The program produces a spectrum by accounting for the contributions from all the individual rotational and atomic lines considered in the calculations. The integrated intensity of each line is distributed in the spectrum by an approximate Voigt profile. The program can produce spectra for either optically thin gases or for cases where simultaneous emission and absorption occur. The method allows calculations ranging from the absorption of incident radiation by a column of cold gas to the high temperature self-absorbed emission spectrum from a nonisothermal gas. The computed spectrum can be output directly and, if desired, the predicted output of a grating spectrograph or a fixed wavelength radiometer can be generated, including instrumental broadening and sensitivity. Several examples illustrating the versatility of the program are presented. Information is given which will enable the reader to acquire a copy of the program and a paper containing instructions for its usage.

INTRODUCTION

THE COMPUTER program described in this paper predicts to good approximation the spectra resulting from electronic transitions of diatomic molecules and atoms. This method is a much expanded and improved version of the program discussed in Ref. 1 and has general application to atomic and all allowed diatomic transitions.

Specifically, the program includes:

1. All parallel transitions ($\Delta\Lambda = \Lambda' - \Lambda'' = 0$), ignoring spin splitting and lambda doubling (ignoring spin splitting and/or lambda doubling means herein that the total multiplet strength is assumed to reside in a single "effective" line).
2. All perpendicular transitions ($\Delta\Lambda = \pm 1$), ignoring spin splitting and lambda doubling.
3. $^2\Pi \leftrightarrow {}^2\Sigma$ transitions, ignoring lambda doubling.
4. Atomic lines.
5. The option to terminate rotational line calculations when a molecule dissociates as a result of rotation.
6. The option to include alternation of line intensity for homonuclear molecules.
7. The use of an approximate Voigt profile for the line shape.
8. Radiative energy transport through multilayers having different thermodynamic properties.

From the above list it is clear that any "allowed" ($\Delta S = 0, \Delta\Lambda = 0, \pm 1$) diatomic transition can be computed to some degree of approximation; however, only the $^1\Sigma \rightarrow {}^1\Sigma$ transitions

are computed exactly. All singlet transitions and the $^2\Pi \leftrightarrow {}^2\Sigma$ transitions are nearly exact since effects of lambda doubling are normally very small. The restrictions on spin splitting and lambda doubling can be removed with a modest reprogramming effort, but this would result in longer computer run times.

The output options available from the program are:

1. The spectral intensity can be printed in tabular form as a function of wavelength.
2. The computed spectrum can be machine plotted.
3. The integrated intensity over an arbitrary number of wavelength intervals can be printed.
4. Curve-of-growth calculations can be printed for an arbitrary number of integration intervals within the computed spectrum.
5. The computed spectrum can be combined with nearly any instrument sensitivity to yield a predicted instrument output, e.g. output voltage for a radiometer. The instrument band pass can be approximated by up to 99 straight line segments or by a Gaussian curve. The instrument sensitivity considered can be either a fixed wavelength band pass to simulate a radiometer or a band pass scanning across any specified wavelength interval. In the latter case the sensitivity can be varied as a function of wavelength to simulate the spectrum that would be recorded by an instrument with linear dispersion (i.e. grating spectrograph). This simulated spectrum can also be machine plotted.

The program is available from COSMIC, Barrow Hall, University of Georgia, Athens, Georgia. The program package includes the program source decks, an 800 BPI magnetic tape with spectroscopic data for 18 diatomic systems, and the input and output for an extensive program checkout. When requesting this program, refer to Flash Sheet number ARC-10217. Additionally, a user's manual has been published in Ref. 2.

THEORY

A real spectrum is often generated by a multitude of overlapping molecular rotational lines, atomic lines, and continua. If it is desired to compute a synthetic spectrum in exact simulation of nature, each of these radiating sources must be considered. The present program is intended to reasonably describe only the molecular rotational lines and atomic lines. The following discussion is limited to the theory of these radiators and is intentionally brief. Detailed information can be found in the references cited.

In order to reasonably compute spectral intensities it is necessary to consider the interaction of the radiation with the particles constituting the gas under consideration. This interaction is discussed in several texts[3,4] and can be seen explicitly in the differential form of the one-dimensional equation of radiative transfer (Ref. 3, p. 460):

$$\frac{dI_\lambda}{dx} = \overbrace{\alpha_\lambda[1-\exp(-hc/\lambda kT)]B_\lambda(T)}^{\text{spontaneous emission}} + \overbrace{\alpha_\lambda I_\lambda \exp(-hc/\lambda kT)}^{\text{induced emission}} - \overbrace{\alpha_\lambda I_\lambda}^{\text{absorption}} \tag{1}$$

$$= \alpha'_\lambda[B_\lambda(T) - I_\lambda]. \tag{2}$$

Equation (1) gives the gradient of the specific intensity, I_λ, W/cm^2-μ-sr, along a given distance x measured from the gas boundary and consists of three basic terms; the first term, giving the spontaneous emission contribution, is independent of the specific intensity.

The remaining terms, giving the contributions due to induced emission and absorption, are proportional to the specific intensity at the point x. The meaning of the remaining symbols in the equation are:

B_λ = Planck black-body function, W/cm^2-μ-sr
α_λ = absorption coefficient, cm^{-1}
$\alpha'_\lambda = \alpha_\lambda[1-\exp(-hc/\lambda kT)]$ = absorption coefficient corrected for stimulated emission, cm^{-1}

Upon integration over x, provided the gas is in thermodynamic equilibrium at a constant temperature T, equation (2) becomes

$$I_\lambda = B_\lambda(T)[1-\exp(-\alpha'_\lambda l)] + I'_\lambda \exp(-\alpha'_\lambda l) \tag{3}$$

where

l = geometric path length, cm
I'_λ = specific intensity incident on gas boundary, W/cm^2-μ-sr.

Equation (3) shows that the parameter needed to compute the spectrum of specific intensity (herein referred to as the "true" spectrum) for a given set of conditions is the absorption coefficient α'_λ. This coefficient is related to the spectral intensity due to spontaneous emission only by Kirchhoff's equation, i.e. $\alpha'_\lambda = E_\lambda/B_\lambda$. The present program first generates the spontaneous emission spectrum E_λ by summing the spectral contributions from all included atomic and rotational lines at many points within the spectral range considered. The points are spaced at equal intervals ($\Delta\lambda$) of a dimension small compared to the narrowest line width considered in the calculation. Then the absorption coefficient at each point is generated by simple division by the black-body function. Finally, the "true" spectrum is generated for a given gas depth and incident radiation source according to equation (3). The program is of great utility because the "true" spectrum for a gas layer can be stored and used as the incident radiation for a new gas layer. This allows the calculation of the "true" spectrum from a multilayer source where each layer is specified by differing thermochemical and thermodynamic properties.

If an optically thin* spectrum is desired as a final result, it is given directly by the spontaneous emission spectrum E_λ. This can be seen by considering equation (3) in the limit as $\alpha'_\lambda l \ll 1$. When the exponential is expanded,

$$I_\lambda|_{\alpha'_\lambda l \ll 1} = \alpha'_\lambda l B_\lambda(T) + I'_\lambda$$

and, equivalently,

$$I_\lambda|_{\alpha'_\lambda l \ll 1} = E_\lambda l + I'_\lambda. \tag{4}$$

The starting point of the procedure then is to compute the spontaneous emission spectrum E_λ. Three fundamental pieces of information are required for each rotational or atomic line to accomplish this task; the location of the line central wavelength λ_{c_L}, the integrated line intensity due to spontaneous emission E, and the appropriate line profile. The first three sections below describe the mathematical expressions used by the program to generate this information for both diatomic molecules and atoms. The two following sections describe further information optionally used in generating the spontaneous

* An optically thin spectrum is a valid approximation to the "true" spectrum, provided $\alpha'_\lambda l \ll 1$ for all wavelengths.

emission spectrum. These are the determination of the maximum rotational quantum number for a given vibrational band and the spectra arising from homonuclear diatomic molecules.

I. *Wavelength of line center*

A. *Atoms.* The central wavelength of each atomic line is input to the program, making a mathematical expression unnecessary. Atomic line wavelengths are tabulated in several sources, e.g. Ref. 5.

B. *Diatomic molecules.* The general expression for the central wavelength of a rotational line is given in Ref. 6 as

$$\bar{\nu} = \nu/c = \bar{\nu}_0(v'v'') + F'(J') - F''(J''), \text{ cm}^{-1} \tag{5}$$

$$\lambda_{\text{Å}} = 10^8/\bar{\nu}, \text{ Å}.$$

The band origin for the (v', v'') transition can either be input directly or computed by the program from the expression

$$\bar{\nu}_0(v'v'') = (T_e' - T_e'') + [G'(v') - G''(v'')] \tag{6}$$

where $G(v)$ is approximated as

$$G(v) = \omega_e(v+\tfrac{1}{2}) - \omega_e x_e(v+\tfrac{1}{2})^2 + \omega_e y_e(v+\tfrac{1}{2})^3 + \omega_e z_e(v+\tfrac{1}{2})^4. \tag{7}$$

The rotational term energy, $F(J)$, is a function of the type of electronic level as well as of J. For singlet transitions the expression for $F(J)$ is given in Ref. 6 as

$$F(J) = F(K) = B_v K(K+1) - D_v K^2(K+1)^2. \tag{8}$$

In the program, this expression is used not only for the singlet transitions but also for all transitions where spin splitting is ignored with the exception of the $\Delta\Lambda = 0$ triplet cases. For these transitions, e.g. C_2(Swan)($^3\Pi_g \rightarrow {}^3\Pi_u$), the central component of the triplet is used as an "effective" line wavelength. Hence, for triplets with $\Delta\Lambda = 0$, the expression used for $F(J)$ is[6]

$$F(J) = F(K) = B_v[K(K+1) + 4Z_2] - D_v(K+\tfrac{1}{2})^4 \tag{9}$$

where

$$Z_2 = \frac{\Lambda^2 Y(Y-1) - \frac{4}{9} - 2K(K+1)}{3[\Lambda^2 Y(Y-4) + \frac{4}{3} + 4K(K+1)]}$$

and $Y = A/B_v$.

When spin splitting cannot be ignored, an accurate expression for $F(J)$ describing the separate levels must be used. For example, the spectrum from $^2\Pi \leftrightarrow {}^2\Sigma$ transitions is poorly represented unless the spin splitting is considered. For these transitions the expressions

used in the program for $F(J)$, ignoring lambda doubling, are

$$\left.\begin{aligned} &\text{for } J = K+\tfrac{1}{2} \\ &\qquad F_1(J) = B_v\{(J+\tfrac{1}{2})^2 - \Lambda^2 - \tfrac{1}{2}\sqrt{[4(J+\tfrac{1}{2})^2 + Y(Y-4)\Lambda^2]}\} \\ &\text{for } J = K-\tfrac{1}{2} \\ &\qquad F_2(J) = B_v\{(J+\tfrac{1}{2})^2 - \Lambda^2 + \tfrac{1}{2}\sqrt{[4(J+\tfrac{1}{2})^2 + Y(Y-4)\Lambda^2]}\} \end{aligned}\right\}. \tag{10}$$

These expressions are given in Ref. 6 with additional terms containing D_v. The higher order terms were ignored here to reduce the number of independent branches from 12 to 8. This point is discussed further on page 781.

II. *Integrated line intensity due to spontaneous emission*

A. *Atoms.* The equation for the integrated intensity due to the spontaneous emission of a single atomic line can be written[6–8] as:

$$E = \frac{\{N_u h\nu A_{ul}\}10^{-7}}{4\pi}, \text{ W/cm}^3\text{-sr} \tag{11}$$

where $N_u = (Nd_u/Q)\exp(-hcT'_e/kT_{\text{elect}})$. The Einstein A coefficients can be found in tabulations, such as in Ref. 5, and the partition function Q for atomic nitrogen and oxygen as well as their ions may be obtained from Ref. 9. As discussed in Ref. 9, the partition function used in the equation for E should be identical to that used in the computation of species concentrations to avoid errors.

B. *Diatomic molecules.* Similarly, the integrated intensity due to spontaneous emission from a single rotational line is given by:

$$E = \left\{\frac{16\pi^3 c N_u \bar{\nu}^4}{3(2J'+1)}\right\}\{|R_e(\bar{r}_{v'v''})|^2 q_{v'v''}\}\{S^{J'\Lambda'}_{J''\Lambda''}\}10^{-7}, \text{ W/cm}^3\text{-sr} \tag{12}$$

where

$|R_e(\bar{r}_{v'v''})|^2$ = square of the electronic transition moment
$q_{v'v''}$ = Franck–Condon factor
$S^{J'\Lambda'}_{J''\Lambda''}$ = line intensity factor, including the rotational degeneracy of the upper state $(2J'+1)$
N_u = number of molecules in the upper state.

Normally, the electronic transition moment cannot be determined for each transition within an electronic multiplet, requiring an average value to be used, i.e.

$$|R_e(\bar{r}_{v'v''})|^2_{\text{av}} = \frac{\Sigma|R_e(\bar{r}_{v'v''})|^2}{d_u} \tag{13}$$

where the summation is over all electronic transitions between the upper and lower multiplet levels. When equation (13) is substituted into (12), the resulting equation for the integrated line intensity due to spontaneous emission agrees with the expression given by NICHOLLS and STEWART.[7] The electronic transition moment is usually a measured quantity

and is related to the often used electronic absorption f-number[10] by

$$\Sigma|R_e(\bar{r}_{v'v''})|^2 = \frac{3hc^2\lambda_{v'v''}d_l f_{el}(\lambda)}{8\pi^2 m_e c}. \tag{14}$$

The f-number or the transition moment can vary with wavelength (or r-centroid), depending on the molecular transition under consideration. Descriptions of the variations of these quantities for some molecules may be found in the literature (see Ref. 10 for a summary article). The Franck-Condon factor, $q_{v'v''}$, and the line strength factor, $S_{J''\Lambda''}^{J'\Lambda'}$ in equation (12) are derivable from theory.

In the above expressions, d is the electronic multiplicity, i.e.

$$d = \delta(2S+1)$$

where

$(2S+1)$ = spin multiplicity

δ = lambda doubling factor; $\delta = 1$ for Σ states, $\delta = 2$ for all other states.

The number of particles in the upper state is given by:

$$N_u = \frac{N d_u (2K'+1)}{Q} \exp\left\{\frac{-hc}{k}\left[\frac{T_e'}{T_{\text{elect}}} + \frac{G'(v')}{T_{\text{vib}}} + \frac{F'(K')}{T_{\text{rot}}}\right]\right\} \tag{15}$$

if the entire electronic multiplet is combined into one "effective" energy level, i.e. spin splitting and lambda doubling are ignored. If spin splitting is considered, such as for the $^2\Pi \leftrightarrow {}^2\Sigma$ transitions, then d_u must be replaced by δ and K' by J'. If spin splitting and lambda doubling are both considered, then d_u must be replaced by 1·0.

The partition function Q for diatomic molecules (see Refs. 11 and 12 for discussions of partition functions) is calculated to good approximation by:

$$Q = \sum_{i=1}^{n}\left\{d_i \exp(-hcT_{e_i}/kT_{\text{elect}})\left\{\sum_{v_j=0}^{v_{j\max}} \frac{kT_{\text{rot}}}{hcB_{v_j}} \exp[(-hc/kT_{\text{vib}})G(v_j)]\right\}\right\}_i. \tag{16}$$

The summation is carried out over all electronic levels of importance for the temperatures considered and over all vibrational levels within each electronic state until either

$$\frac{\exp[(-hc/kT_{\text{vib}})G(v_{j_{\max}})]}{\Sigma_{v_j}\exp[(-hc/kT_{\text{vib}})G(v_j)]} \leq 0{\cdot}001$$

or the equation representing the vibrational energy [equation (7)] has reached a fictitious peak, i.e. $G(v_{\max}+1) \leq G(v_{\max})$. In the interest of accuracy and consistency, when predicted diatomic species concentrations are used with the present program, one should check to see that the partition function used in those calculations gives results equivalent to those of equation (16).

Note that specifying the electronic, vibrational, and rotational temperatures separately in equations (15) and (16) allows for the assumption that each energy mode is populated with a different Boltzmann distribution.

The line strength factor, $S_{J''\Lambda''}^{J'\Lambda'}$, depends on the type of electronic transition and the spin multiplicity as well as J. As noted in the Introduction, three types of electronic transitions are considered in the program, but spin multiplicity is considered only for the $^2\Pi \leftrightarrow {}^2\Sigma$

transitions. The expressions for the line strength factors used for each of these cases are discussed below.

1. *Parallel transitions* ($\Delta\Lambda = 0$). These transitions are characterized by strong P and R branches and other weak branches that die out rapidly with increasing quantum number. Spin splitting is ignored for these transitions in the program and the strength factors are assigned as for the ${}^1\Sigma \rightarrow {}^1\Sigma$ case as given in Ref. 6, i.e.

$$\left.\begin{aligned} P \text{ branch}: S^{K'\Lambda'}_{K''\Lambda''}(P) &= K'+1 \\ R \text{ branch}: S^{K'\Lambda'}_{K''\Lambda''}(R) &= K' \end{aligned}\right\}. \tag{17}$$

By this assignment the weak branches are assumed to have zero intensity. However, this missing intensity is assigned to the P and R branches, because the sum of the strength factors for any K' obeys the sum rule $\Sigma_{K''} S^{K'\Lambda'}_{K''\Lambda''} = 2K'+1$. It is interesting that in the limit of high K values these strength assignments are exact regardless of spin.

2. *Perpendicular transitions* ($\Delta\Lambda = \pm 1$). These transitions are characterized by strong Q branches and slightly weaker P and R branches. If the resultant electron spin is zero, these are the only branches. If the resultant electron spin is nonzero, then, as above, other weak branches exist, but die out rapidly with increasing quantum number. Only the singlet strength factors are used in the program and were taken from Ref. 13.

$$\left.\begin{aligned} P \text{ branch}: S^{K'\Lambda'}_{K''\Lambda''}(P) &= \frac{(K'+1\mp\Lambda')(K'+2\mp\Lambda')}{2(K'+1)} \\ Q \text{ branch}: S^{K'\Lambda'}_{K''\Lambda''}(Q) &= \frac{(K'\pm\Lambda')(K'+1\mp\Lambda')(2K'+1)}{2K'(K'+1)} \\ R \text{ branch}: S^{K'\Lambda'}_{K''\Lambda''}(R) &= \frac{(K'\pm\Lambda')(K'-1\pm\Lambda')}{2K'} \end{aligned}\right\}. \tag{18}$$

Here the upper sign is for $\Delta\Lambda = \Lambda' - \Lambda'' = +1$ and the lower sign is for $\Delta\Lambda = -1$. The arguments given above concerning the weaker branches in the parallel transitions are also applicable for the perpendicular transitions.

3. ${}^2\Pi \leftrightarrow {}^2\Sigma$ *transitions*. These transitions exhibit 12 possible branches, corresponding to $\Delta J = 0, \pm 1$ and $\Delta K = 0, \pm 1, \pm 2$, and all must be considered. If the D_v terms are not included in the rotational term energy equation [equation (10)], the rotational lines from 4 of the branches have exactly the same wavelength as 4 other branches and the number of distinct branches is reduced to 8. The "effective" strength of these double lines is found by summing the two separate strength factors. The following table lists the single and double branches that result in emission.

The strength factors of these branches for any degree of coupling between Hund's case *a* and case *b* were developed by EARLS.[14] However, if Earls' line strengths are summed for all the transitions from (or to) a given rotational level, i.e.

$$S(P_2) + S({}^QP_{21}) + S(Q_2) + S({}^RQ_{21}) + S(R_2) + S({}^SR_{21})$$

or

$$S({}^OP_{12}) + S(P_1) + S({}^PQ_{12}) + S(Q_1) + S({}^QR_{12}) + S(R_1)$$

the sum is $(2J+1)/2$ rather than the required $(2J+1)$. The strength factors used in the program (Table 2) are, therefore, the expressions given by Earls multiplied by 2·0. The Λ and J values in the strength factors are for the $^2\Pi$ state.

TABLE 1

8 distinct branches resulting for	
$^2\Pi$ upper state	$^2\Sigma$ upper state
P_2	R_2
R_1	P_1
$^SR_{21}$	$^SR_{21}$
$^OP_{12}$	$^OP_{12}$
Q_2 and $^QP_{21}$	Q_2 and $^QR_{12}$
Q_1 and $^QR_{12}$	Q_1 and $^QP_{21}$
R_2 and $^RQ_{21}$	P_2 and $^PQ_{12}$
P_1 and $^PQ_{12}$	R_1 and $^RQ_{21}$

TABLE 2

Transition		Strength factor
$^2\Pi \rightarrow {}^2\Sigma$	$^2\Sigma \rightarrow {}^2\Pi$	
P_2	R_2	$\dfrac{(2J+1)^2+(2J-1)U(4J^2+4J+1-2Y)}{16(J+1)}$
$^OP_{12}$	$^SR_{21}$	
$^QP_{21}$	$^QR_{12}$	$\dfrac{(2J+1)^2+(2J+1)U(4J^2+4J-7+2Y)}{16(J+1)}$
P_1	R_1	
Q_2	Q_2	$\dfrac{(2J+1)[(4J^2+4J-1)\pm U(8J^3+12J^2-2J+1-2Y)]}{16J(J+1)}$
$^PQ_{12}$	$^RQ_{21}$	
$^RQ_{21}$	$^PQ_{12}$	$\dfrac{(2J+1)[(4J^2+4J-1)+U(8J^3+12J^2-2J-7+2Y)]}{16J(J+1)}$
Q_1	Q_1	
R_2	P_2	$\dfrac{(2J+1)^2+(2J+1)U(4J^2+4J-7+2Y)}{16J}$
$^QR_{12}$	$^QP_{21}$	
$^SR_{21}$	$^OP_{12}$	$\dfrac{(2J+1)^2\mp(2J+1)U(4J^2-4J+1-2Y)}{16J}$
R_1	P_1	

Here, the upper sign goes with the upper listed branch and $Y = A/B_v$,

$$U = [Y^2 - 4Y + (2J+1)^2]^{-1/2}.$$

III. *Line shape*

The line shape is assumed to be adequately approximated by the Voigt profile. Reference 15 gives a closed-form approximation of the Voigt profile that lends itself to rapid calculation and is generally accurate to within 3 per cent or less. This approximation* was used in the program and the appropriate equations are listed below:

$$E_\lambda = E_{\lambda_{\mathbf{Q}}}\left\{\left(1-\frac{w_l}{w_v}\right)\exp\left[-2{\cdot}772\left(\frac{\lambda-\lambda_{\mathbf{Q}}}{w_v}\right)^2\right]+\frac{w_l/w_v}{1+4[(\lambda-\lambda_{\mathbf{Q}})/w_v]^2}\right.$$
$$\left.+0{\cdot}016\left(1-\frac{w_l}{w_v}\right)\left(\frac{w_l}{w_v}\right)\left\{\exp\left[-0{\cdot}4\left(\frac{\lambda-\lambda_{\mathbf{Q}}}{w_v}\right)^{2{\cdot}25}\right]-\frac{10}{10+[(\lambda-\lambda_{\mathbf{Q}})/w_v]^{2{\cdot}25}}\right\}\right\} \quad (19)$$

$$E_{\lambda_{\mathbf{Q}}} = \frac{E}{w_v[1{\cdot}065+0{\cdot}447(w_l/w_v)+0{\cdot}058(w_l/w_v)^2]}, \qquad w_v = \frac{w_l}{2}+\sqrt{[(w_l/2)^2+w_g^2]}.$$

Here, E_λ is the spectral intensity at any value of λ, $E_{\lambda_{\mathbf{Q}}}$ is the value at the line center, and w_v, w_l, and w_g are the Voigt, Lorentzian, and Gaussian line widths at half-height.

Given w_l and w_g, the Voigt profile is determined and the line is added into the spontaneous emission spectrum for a specified number of line widths from the line center. This specification can be made in one of two ways. When the "true" spectrum is heavily absorbed, and the spectral region of interest is far from the center of any spectral line, the far wings of the nearest lines must be considered. In this case the distance to which the wings will be computed should be specified in the program input for the appropriate lines. However, placing the termination point at large distances from the line center for an extensive number of lines can significantly increase the computer run time.

In regions where the "true" spectrum contains large numbers of closely spaced lines (i.e. within a band sequence) or for optically thin gases, the far wings of the lines are not very important. In these cases input data specifying the termination distance can be left blank and the program will set the distance according to the specified line shape. For a pure Gaussian line profile ($w_l = 0$), $E_\lambda/E_{\lambda_{\mathbf{Q}}}$ is negligible ($<10^{-11}$) 3 line widths from the line center and the line is terminated at this point. For a Lorentzian or Voigt line profile ($w_l \neq 0$) the far wings of the line are more intense and the line is terminated 5 line widths from the line center. In the worst case (pure Lorentzian, $w_g = 0$) approximately 5 per cent of the spontaneous integrated line intensity lies beyond this termination point and is not included in the calculation.

IV. *Determination of maximum rotational quantum number*

Since the program computes diatomic spectra line by line, there must be some criterion for choosing the number of rotational lines considered in the calculation. The user can make this choice by specifying the minimum and maximum rotational quantum numbers

* A very accurate computer solution for the Voigt profile has been written by C. Young of the University of Michigan. However, the approximation used herein requires less machine storage and is appreciably faster than the "exact" program. For example, the approximation is about 2 times faster for a pure Lorentzian line, about 3 times faster for a pure Gaussian line, and about 250 times faster for a line with nearly equal Gaussian and Lorentzian widths. The overall computer run time is roughly proportional to the number of lines considered. Therefore, using the approximation reduces run time and expense by roughly the appropriate factors given above with only a small loss of accuracy in the spectral calculation.

desired for each vibrational transition. However, the program can also compute the maximum rotational quantum number possible before the molecule dissociates as a result of rotation. The method for finding the maximum rotational quantum number is similar to that discussed in Refs. 6 and 12. The effective potential energy of the rotating system is taken to be the sum of the rotational term and a Morse potential.

V. *Spectra of homonuclear diatomic molecules*

The bands of homonuclear molecules exhibit a characteristic alternation in line intensity. In some cases every other line is entirely missing because the nuclear spin changes the multiplicity or statistical weight of the rotational levels as described in Ref. 6. This precept can be stated mathematically and is used in the program as:

$$E' = E\left[1 + \frac{(-1)^{K''+C}}{2I+1}\right]. \tag{20}$$

Here

E' = adjusted integrated line intensity
E = integrated line intensity from equation (12)
I = nuclear spin of each atom
C = integer that specifies the stronger lines.

If C is even the lines with even K'' are stronger. Whether the odd or even lines are stronger can be determined from the discussion on pp. 167 and 168 of Ref. 13.

PROGRAM CHECK OUT AND EXAMPLE CALCULATIONS

A computer program is obviously only as good as the theoretical model on which it is based and the accuracy with which the mathematical expressions of the model are translated into computer instructions. The prior section has defined the model and discussed the important assumptions made in this application. The main purpose of this section is to demonstrate that the program computes spectra as intended and to give sample calculations illustrating its usefulness and versatility.

Before starting it is interesting to note that the computer run time is determined mainly by the time required to generate the spontaneous emission spectrum. This time can be predicted by an equation of the form

Run time $\approx$ (constant) (total number of included lines) (number of line widths to termination point of line) $(w_v/\Delta\lambda)$, minutes.

For the IBM 7094 computer used in the present work, the value of the constant is $5{\cdot}8 \times 10^{-5}$ minute/line. Run times for a few sample calculations will be given below.

I. *Wavelength of line center*

The accuracy of the expression for wavelength, equation (5), was checked by comparing the computed results for several band systems with experimental measurements.[16,17]

Specific results are shown in Fig. 1 where the computed band-head wavelengths for the CN (red) ($A^2\Pi \rightarrow X^2\Sigma$) transition are compared to the measurements of Ref. 17. The computed wavelengths of the four band heads for each (v', v'') transition were subtracted

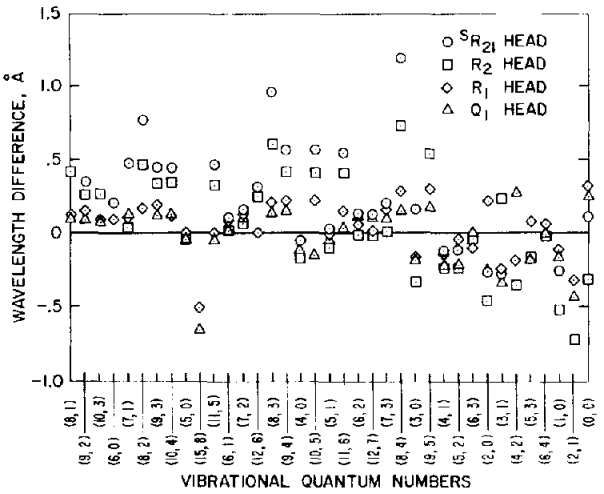

FIG. 1. Difference between measured and computed band-head wavelengths for the CN (red) ($A^2\Pi \rightarrow X^2\Sigma$) transition.

from the available data and this difference is plotted against the band vibrational quantum numbers. The band quantum numbers are ordered with respect to increasing wavelength and include the region from about 4800 to 11 000 Å. The spectroscopic constants used in the computation were taken from Refs. 6 and 18. Generally, the differences are 0·5 Å or less over a wide range of wavelength and vibrational quantum numbers which is strong evidence that the forms of equations (5), (6), and (10) are programmed correctly.

Here known spectroscopic constants and measured wavelengths have been used to check the program. Alternatively, note that if new measured wavelengths were in hand, the program could be of great use in determining the appropriate new spectroscopic constants.

II. *Optically thin integrated intensity*

The accuracy of the expression for the integrated line intensity due to spontaneous emission, equation (12), was checked by comparing optically thin integrated band intensities for a 1-cm path length with values given by the "Q-branch" theory.[19] "Q-branch" theory does not yield detailed band structure but does give good results for the optically thin integrated intensity from a band or a band sequence.

The comparison shown in Fig. 2 and Table 3 was made for the prominent spectral features in a 50 per cent CO_2–50 per cent N_2 gas mixture heated to 6000°K, with density, ρ/ρ_0, of 10^{-2}. The upper curve in Fig. 2 is the result of the present work and the lower curve is the result from "Q-branch" theory. The present work shown in this figure as well as that in the following figures was machine plotted using the Ames plot routine. In this technique, each computed point is connected to its neighbor by a straight-line segment. In the regions of band system overlap, the "Q-branch" theory was plotted as the sum of the contributing systems to allow comparison with the present results. The band systems considered were the CN (violet) ($B^2\Sigma \rightarrow X^2\Sigma$), CN (red) ($A^2\Pi \rightarrow X^2\Sigma$), and C_2 (Swan) ($A^3\Pi_g \rightarrow X^3\Pi_u$) transitions and the species concentrations were taken from Ref. 19.

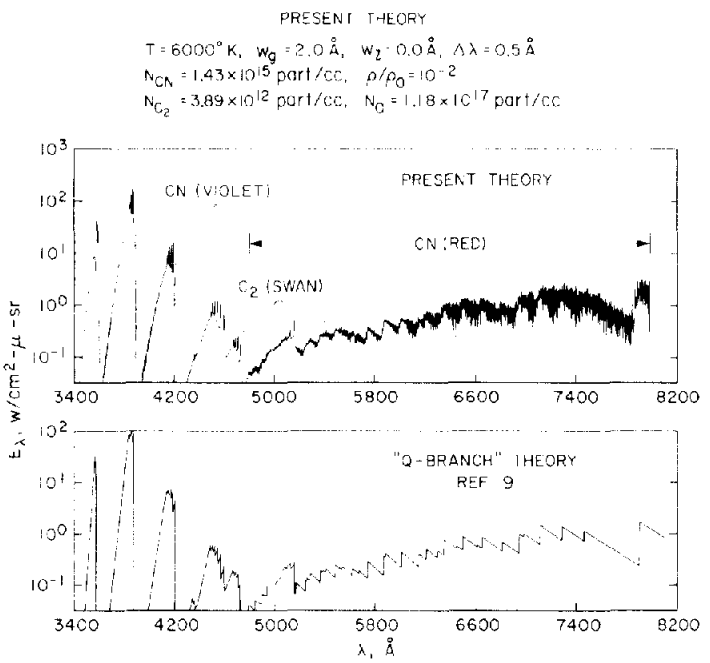

FIG. 2. Comparison of present optically thin calculations with "Q-branch" theory for a 1-cm-thick slab of a heated 50 per cent CO_2 50 per cent N_2 gas mixture in thermochemical equilibrium.

The square of the dimensionless transition moment, $\Sigma|R_e(\bar{r}_{v'v''})/ea_0|^2$, was assumed constant for each band system and the values used were 0·56, 0·52, and 3·56, respectively. The Franck–Condon factors were taken from Ref. 20, the spectroscopic constants of CN were taken from Refs. 6, 18, and 21. The spectroscopic constants for C_2 (Swan) were taken from Ref. 22. Line shapes for the line-by-line calculations were specified as pure Gaussian profiles with $w_g = 2{\cdot}0$ Å. The atomic oxygen triplet near 7774 Å is also included in the line-by-line calculation, but at these conditions the lines are too weak to show above the CN (red) structure. This example illustrates the large number of rotational lines in diatomic spectra as there are 68 100 individual rotational lines and 3 atomic lines represented in the figure. The computer run time for this case was 50 min.

Table 3 gives typical comparisons of the optically thin integrated intensities from various bands of the three systems. The integration for each branch was terminated at the 150th rotational line because the calculations indicated that very little band energy exists beyond this point. For comparison, the "Q-branch" integrations were performed over comparable wavelength intervals. The bands chosen for comparison were purposely taken from widely separated spectral positions to check for differences depending on wavelength. The comparison of integrated intensities is generally good, the largest differences occurring for the CN (red) system. This result is reasonable because the CN (red) structure is quite complex and the "Q-branch" results are not as precise for this system, tending to give values slightly higher than the present work. Also in Table 3 note that the present calculations agree with those of Ref. 9 for the optically thin integrated line intensities from the atomic oxygen triplet, indicating that equation (11) was programmed properly.

TABLE 3. COMPARISON OF OPTICALLY THIN INTEGRATED INTENSITIES FOR A 1-CM PATH LENGTH

(v', v'')	Q-branch theory,[19] $E_{v'v''}$, W/cm^2-sr	Present work $E_{v'v''}$, W/cm^2-sr	Ratio of $E_{v'v''}$ for present work to Q-branch
	CN (violet)		
(3, 2)	$2{\cdot}22^{-2}$	$2{\cdot}19^{-2}$	0·986
(1, 0)	$2{\cdot}53^{-2}$	$2{\cdot}51^{-2}$	0·991
(4, 4)	$2{\cdot}66^{-2}$	$2{\cdot}65^{-2}$	0·994
(0, 0)	$3{\cdot}08^{-1}$	$3{\cdot}07^{-1}$	0·996
(5, 6)	$4{\cdot}18^{-3}$	$4{\cdot}15^{-3}$	0·994
(0, 1)	$2{\cdot}07^{-2}$	$2{\cdot}06^{-2}$	0·991
(5, 7)	$8{\cdot}96^{-4}$	$8{\cdot}87^{-4}$	0·990
(0, 2)	$1{\cdot}22^{-3}$	$1{\cdot}21^{-3}$	0·989
	C_2 (Swan)		
(4, 2)	$8{\cdot}67^{-5}$	$8{\cdot}52^{-5}$	0·982
(2, 0)	$4{\cdot}61^{-5}$	$4{\cdot}53^{-5}$	0·983
(5, 4)	$1{\cdot}93^{-4}$	$1{\cdot}89^{-4}$	0·979
(1, 0)	$4{\cdot}94^{-4}$	$4{\cdot}84^{-4}$	0·980
(2, 2)	$1{\cdot}65^{-4}$	$1{\cdot}62^{-4}$	0·978
(0, 0)	$1{\cdot}63^{-3}$	$1{\cdot}59^{-3}$	0·978
(4, 5)	$6{\cdot}76^{-5}$	$6{\cdot}59^{-5}$	0·976
(0, 1)	$3{\cdot}41^{-4}$	$3{\cdot}33^{-4}$	0·977
	CN (red)		
(8, 1)	$3{\cdot}57^{-4}$	$3{\cdot}13^{-4}$	0·877
(9, 2)	$7{\cdot}36^{-4}$	$6{\cdot}49^{-4}$	0·882
(8, 2)	$2{\cdot}19^{-3}$	$1{\cdot}95^{-3}$	0·892
(9, 3)	$2{\cdot}80^{-3}$	$2{\cdot}53^{-3}$	0·901
(12, 6)	$2{\cdot}11^{-3}$	$1{\cdot}92^{-3}$	0·908
(4, 0)	$5{\cdot}98^{-3}$	$5{\cdot}43^{-3}$	0·907
(4, 1)	$2{\cdot}87^{-3}$	$2{\cdot}65^{-2}$	0·922
(0, 0)	$1{\cdot}30^{-1}$	$1{\cdot}24^{-1}$	0·955
	Atomic oxygen		
$\lambda_{c.}$, Å	Ref. 9 E, W/cm^2-sr	Present work E, W/cm^2-sr	Ratio of E for present work to Ref. 9
7772·0	$6{\cdot}06^{-5}$	$6{\cdot}06^{-5}$	1·0
7774·2	$4{\cdot}33^{-5}$	$4{\cdot}33^{-5}$	1·0
7775·4	$2{\cdot}60^{-5}$	$2{\cdot}60^{-5}$	1·0

Note: The superscript on a number indicates the appropriate power of 10, e.g. $3{\cdot}3^{-5} = 3{\cdot}3 \times 10^{-5}$.

III. *Calculations of "true" spectra from single hot gas layers and molecular curves of growth*

Results obtained from use of the computed spontaneous emission spectrum and the expression for radiative transfer, equation (3), were tested against the line-by-line

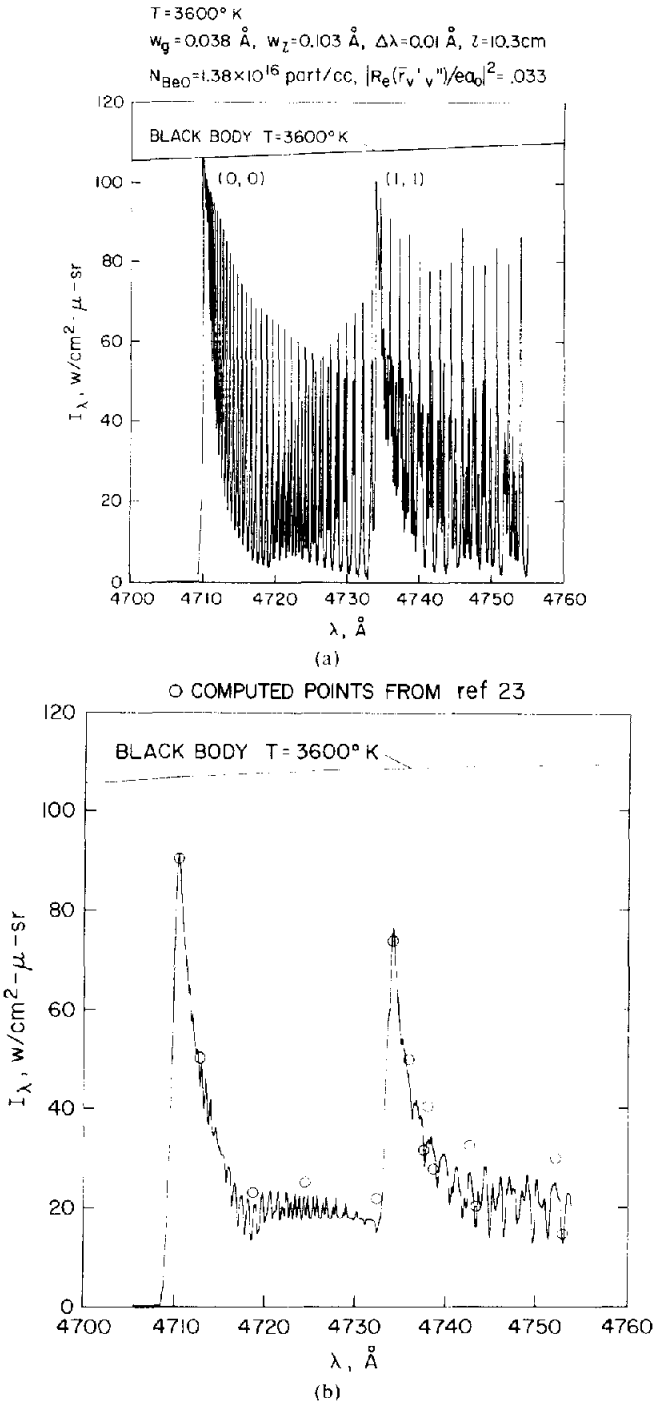

FIG. 3. Self-absorbed BeO ($^1\Sigma \rightarrow {}^1\Sigma$) spectrum in the region of the (0, 0) and (1, 1) band heads. (a) Spectrum without instrumental broadening, (b) Spectrum of Fig. 3(a) as seen through a grating spectrograph and comparison of present self-absorbed calculations with those of Ref. 23.

BeO($^1\Sigma \rightarrow {}^1\Sigma$) calculation reported by DRAKE, TYTE and NICHOLLS.[23] Their calculations do not account for induced emission, but in this case the correction is quite small and can be ignored. The calculation also allowed a check of the Voigt line profile approximation and the capability of the program to produce a spectrum as seen through a grating spectrograph.

Figure 3(a) shows the "true" spectrum without instrumental broadening. In this calculation, the spectroscopic constants were taken from Ref. 6 and the Franck–Condon factors from Ref. 23. The dimensionless electronic transition moment $|R_e(\bar{r}_{v'v''})/ea_0|^2$ was taken as $3{\cdot}31 \times 10^{-2}$, the path length as 10·3 cm, the gas temperature as 3600°K, and the BeO species concentration as $1{\cdot}38 \times 10^{16}$ part/cc. The line widths were input as $w_g = 0{\cdot}038$ Å and $w_l = 0{\cdot}103$ Å and the resulting Voigt width w_v is 0·116 Å. These input data are the same as those used in Ref. 23. Note in Fig. 3(a) that the peak of the (0, 0) R branch just touches the 3600°K black-body limit curve drawn on the figure. The computer run time for this case was 2 min.

Figure 3(b) shows the spectrum of Fig. 3(a) as it would be seen through a grating spectrograph with a 1·2 Å wide rectangular slit function with a peak response of unity. The circles show points read from the comparable synthetic spectrum of Ref. 23 using their 3600°K black-body curve as a reference (apparently a factor of 10^{-3} was lost from the intensity scale of the reference figure in reproduction). The agreement is quite good, with the only noticeable differences occurring far from the band heads.

The above comparison was for a $^1\Sigma \rightarrow {}^1\Sigma$ transition in which spin splitting is not involved. However, in many transitions, spin splitting is present and neglecting it can lead to significant errors in the calculation of heavily self-absorbed spectra. The obvious way to correct for spin splitting is to make the necessary changes in the program and compute each line separately as was done for the $^2\Pi \rightarrow {}^2\Sigma$ transitions. Unfortunately, this lengthens the computer run times. Another way to account for spin splitting is to choose an effective line shape that results in a peak intensity close to that found within the true multiplet. Two limiting cases are considered: (1) When the spin separation is small compared to the line width and the lines merge into a single line. This is representative of the situation in the present program when spin splitting is ignored. (2) When the spin separation is large compared to the line width. In this case the lines are not significantly overlapped, and the peak intensity at the line center is given to good approximation by using an "effective" line width equal to the normal width multiplied by the spin multiplicity. This has the effect of smearing the line to approximate the true multiplet rather than adding the intensities. For intermediate cases selecting an effective width is more difficult.

To evaluate the differences between the two limiting cases C_2 (Swan) ($^3\Pi_g \rightarrow {}^3\Pi_u$) curve-of-growth (integrated specific intensity versus product of particle concentration and path length) calculations at 7000°K were made for the integrated intensity falling between the (0, 0) and (1, 1) band heads. These calculations were compared to the computations by FAIRBAIRN,[24] which accounted for the triplet splitting. The comparison using fully overlapped lines is shown in Fig. 4(a) and using nonoverlapped lines in Fig. 4(b). In the region of heavy self-absorption, the calculation using fully overlapped lines is in poor agreement with Fairbairn's results. However, the calculations for the nonoverlapped lines using an "effective" line width three times (i.e. the spin multiplicity) the line width specified by Fairbairn is in good agreement with his results. The maximum disagreement for the cases considered ($a = 1{\cdot}0$ and 0·01) is 6 per cent. The parameter a relates the Gaussian and

Lorentzian line widths and is defined in the symbols list and on Fig. 4(a). The computer run time for a C_2 (Swan) curve of growth was typically 4 min.

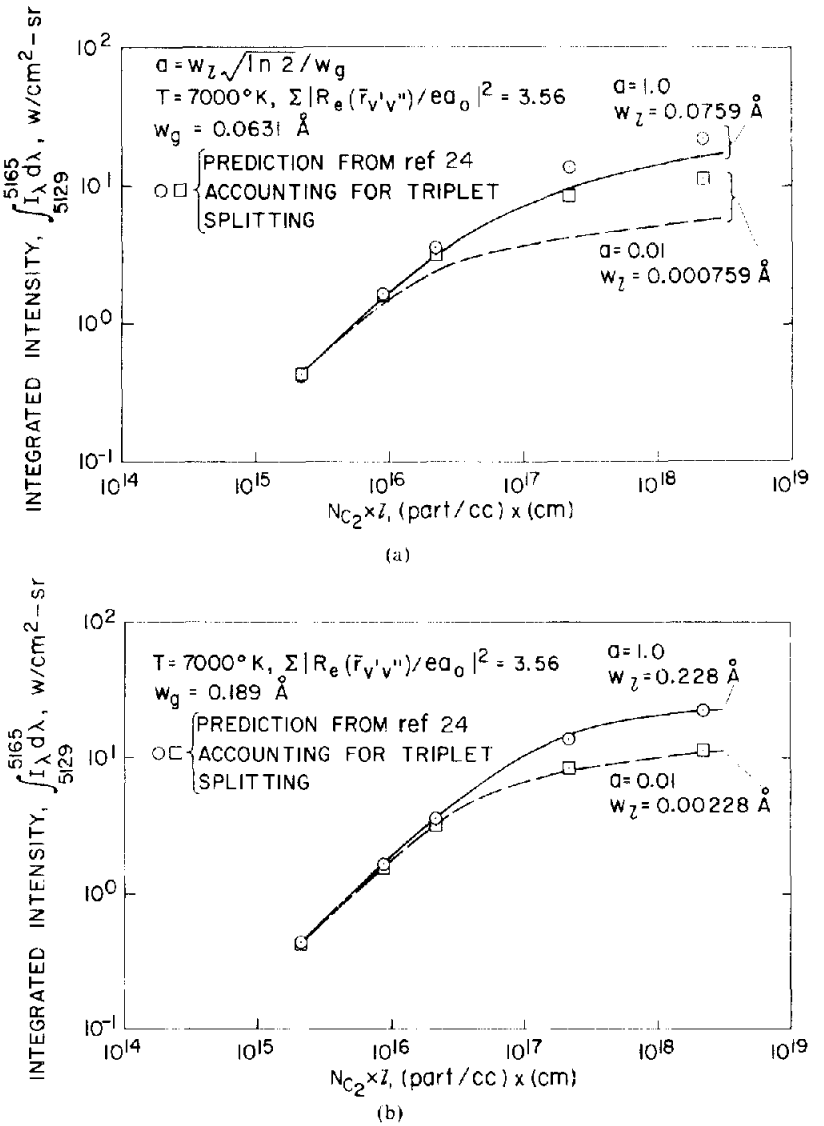

FIG. 4. Effect of limiting treatments of spin splitting on the C_2 (Swan) curve of growth. (a) Comparison between present work and Ref. 24 for the integrated intensity falling between the (0, 0) and (1, 1) band heads (limiting case where multiplet lines are assumed to be fully overlapped in the present work). (b) Limiting case where multiplet lines are assumed not to be significantly overlapped in the present work.

The following examples further demonstrating possible applications of the program are thought to be new contributions; consequently, no comparison data are presented.

The first of these is shown in Fig. 5 and illustrates the approach of CO(4+) ($^1\Pi \rightarrow {}^1\Sigma$) emission to the black-body limit as the geometrical depth of radiating gas is increased. The bands in the region from 1440 to 1700 Å were considered and the CO concentration is that for a 50 per cent CO_2–50 per cent argon gas mixture heated to 6000°K at a density, ρ/ρ_0, of 10^{-2}.[19] In this calculation all lines have been computed with $w_g = 1{\cdot}0$ Å and $w_l = 0$ Å. Since this is a singlet transition, corrections for spin splitting are not required.

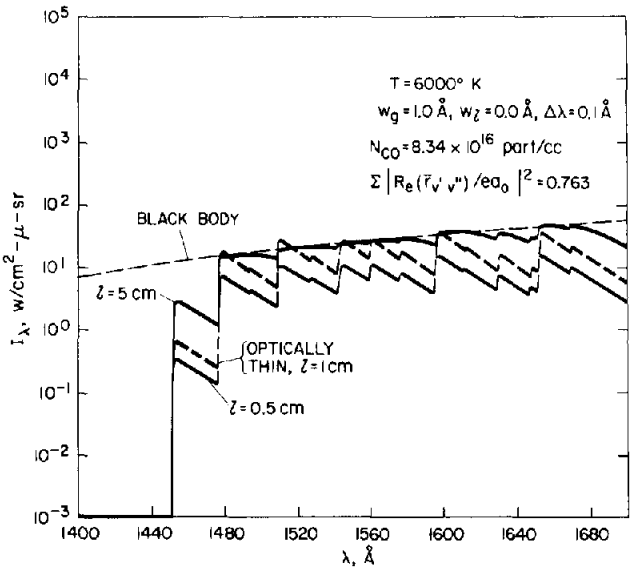

FIG. 5. Comparison of CO (4+) ($^1\Pi \rightarrow {}^1\Sigma$) self-absorbed and optically thin spectra.

Further, the square of the dimensionless transition moment for all (v', v'') transitions was taken as 0·76 corresponding to an electronic absorption f-number of 0·15 at 1545 Å. The Franck–Condon factors were taken from Ref. 25 and the spectrographic constants from Ref. 6. Notice that at a depth of 5 cm the "true" spectrum is approaching the 6000°K black-body curve drawn on the figure. Also note that the 1·0-cm path length, optically thin spectrum (dashed lines) actually exceeds the black-body limit in several places.

Calculations similar to those shown in Fig. 5 were used to produce the CO (4+) curve of growth shown in Fig. 6. The calculations for the integrated intensity falling between the (0, 0) and (4, 3) band heads were made with a Gaussian line width of 0·0162 Å computed from the elementary doppler width formula (see symbols list) and line width parameters, a, of 1·0 and 0·01. The choice of a was arbitrary as it is beyond the scope of the present paper to discuss dispersive line widths. All other parameters used for the curve-of-growth calculations are the same as those of Fig. 5. Since the CO (4+) bands are closely spaced and degraded to the red, considerable intensity in the integration interval comes from the tails of the bands located to the violet of the (0, 0) band heads. This contribution was included by considering all bands 200 Å to the violet of the (0, 0) band in the calculations. The tail of the

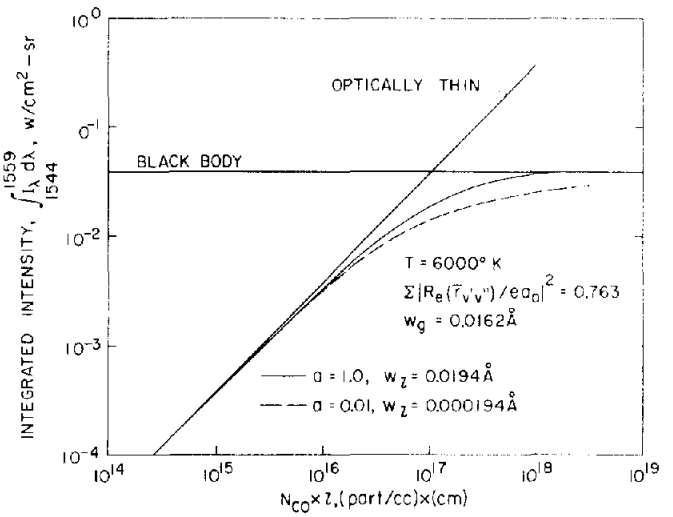

FIG. 6. CO (4 ·) curve of growth for the integrated intensity falling between the (0, 0) and (4, 3) band heads.

next band beyond this point would have contributed less than 0·05 per cent to the spontaneous emission in the integration interval as determined in an auxiliary calculation. The computer run time for each curve of growth was typically 12 min.

The final "true" spectrum from a single hot gas layer is shown in Fig. 7 with and without instrumental broadening by an instrument with linear dispersion (i.e. grating spectrograph). The source was taken to be a 1-cm-thick slab of gas with a temperature of 6000°K and CN species concentration of $1{\cdot}0 \times 10^{15}$ part/cc. An arbitrarily high atomic nitrogen concentration of $2{\cdot}0 \times 10^{21}$ atoms/cc was assumed to make the two nitrogen lines near 10 880 Å visible above the CN (red) structure. The input data necessary to compute the integrated intensity due to spontaneous emission from the nitrogen lines were taken from Ref. 9 and the spectroscopic constants for CN (red) were identical to those of Fig. 1. The Gaussian line widths for the CN and N transitions were input as the Doppler width values for 6000°K and in both instances the line width parameter was assumed to be 1·0. All other CN input data were identical with those used in Fig. 2.

Note that the locations of the four (0, 0) CN (red) band heads are indicated on the figure. Except for the arbitrarily strong nitrogen lines, this calculation is representative of the spectrum that might be observed by looking from the stagnation point normal to the shock layer of a blunt body flying in a possible Mars atmosphere. The normalized slit function of the grating instrument yielding the broadened spectrum was taken as a rounded-corner trapezoid and is shown in Fig. 7(b). The spectral calibration of this instrument was assumed to be wavelength dependent according to the curve also shown in Fig. 7(b). The computer run time for this case was 2·4 min.

IV. *Cold gas absorption spectra*

Another application of the program is to generate cold gas absorption spectra. Figure 8, illustrating this capability, shows the extinction of the incident radiation by a 10-cm-thick

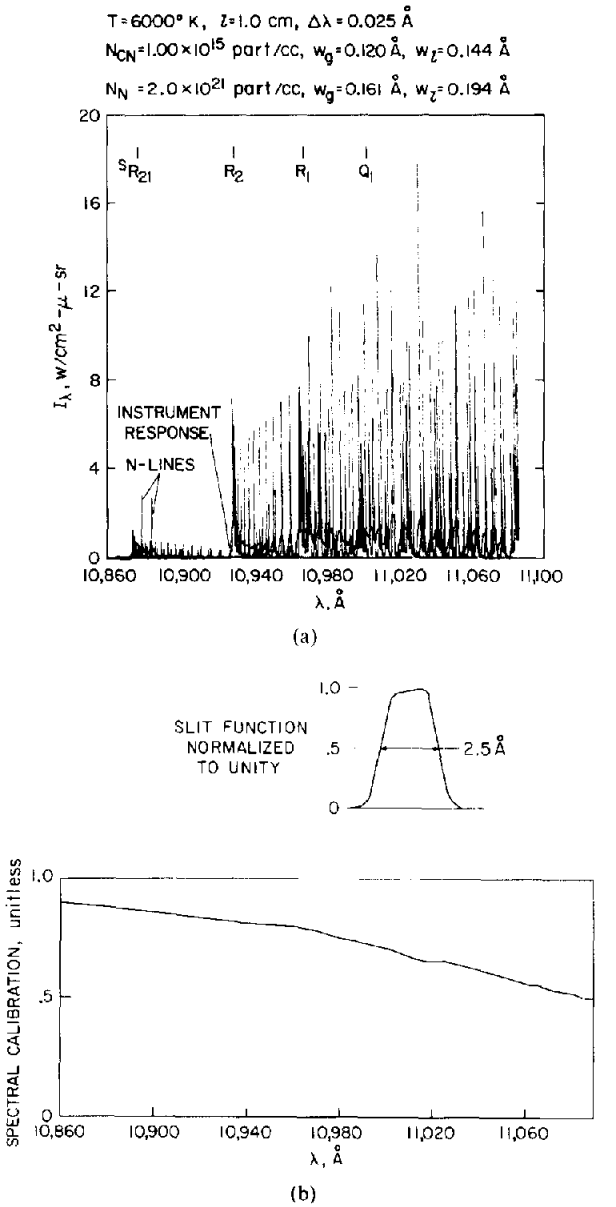

FIG. 7. "True" spectrum of atomic nitrogen and CN (red) in the region of the (0, 0) band heads. (a) Spectrum with and without instrument broadening. (b) Curves specifying instrument calibration used in Fig. 7(a).

gas layer having a CO concentration of $1{\cdot}0 \times 10^{15}$ part/cc. The incident radiation was assumed to be from a 6000°K black body. The other parameters and bands considered are the same for this case as those of Fig. 5, except that the gas temperature was taken as 300°K.

Note that because of this low temperature only the (2, 0), (1, 0), and (0, 0) bands show noticeable absorption, and that the extent of the rotational population within these bands is quite limited. In the absorbed regions, the incident radiation curve is shown as a dashed line.

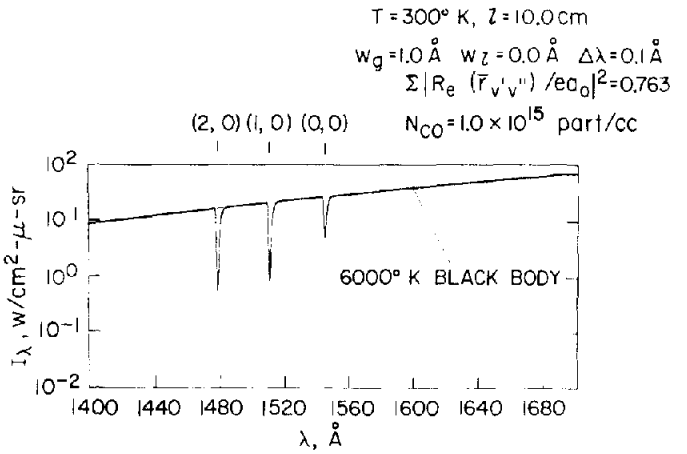

FIG. 8. CO (4 +) cold gas absorption of a 6000°K black-body incident spectrum.

V. *Nonisothermal calculations*

The final feature of the program to be demonstrated is its capability to generate the "true" spectrum produced by a source consisting of several gas layers, each specified by a different composition and temperature.

This example is for two layers only, but, as noted before, the number of layers the program can consider is arbitrary. The first layer of the source was taken to be 1 cm thick with a temperature of 6000°K and a CO concentration of $8{\cdot}34 \times 10^{15}$ part/cc. The only transition considered was the CO (4 +) (0, 0) band and the line widths and other pertinent input data were identical to the $a = 1{\cdot}0$ case of Fig. 6. The upper portion of Fig. 9 shows the spectrum emitted from this layer in the region of the (0, 0) band heads; the input data pertinent to this layer are listed beside the spectrum.

The second layer was taken to be a 10-cm-thick slab with a CO concentration of $1{\cdot}0 \times 10^{15}$ part/cc at a temperature of 1000°K. All other input data except for the line widths were the same as those of the first layer. The Gaussian line width was used as the doppler value for 1000°K and again the line width parameter was chosen as 1·0. The lower portion of the figure shows the "true" spectrum from both layers of the source and illustrates a dramatic reduction in specific intensity by absorption in the cooler layer. Specifically note that the centers of the high emission peaks from the first layer are strongly absorbed by the narrower lines in the second layer, leaving two emission peaks, one on each side of the location of the original peak. The total computer run time for Fig. 9 was 1·9 min.

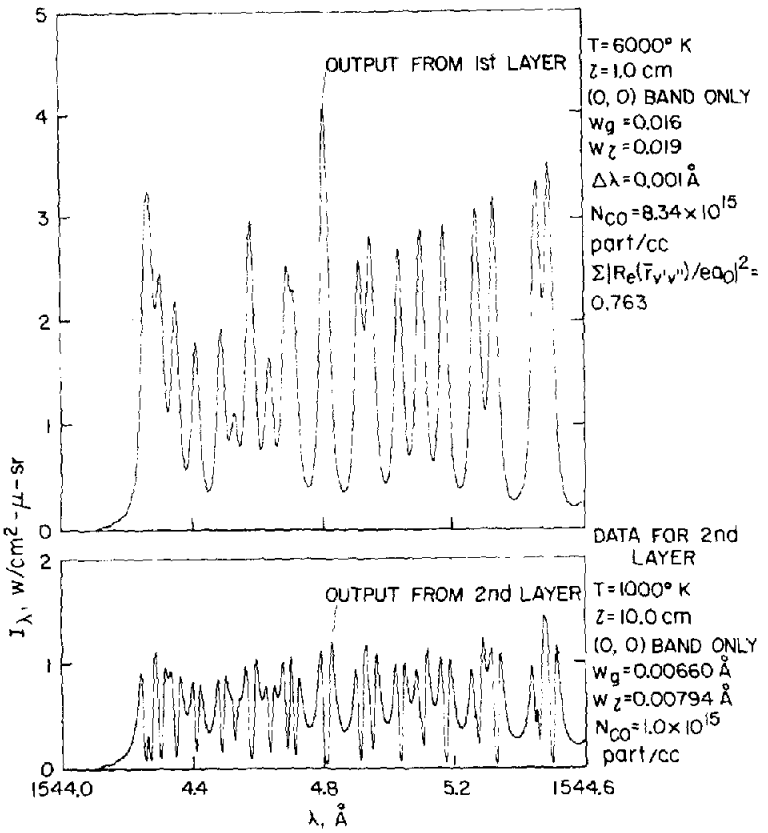

FIG. 9. "True" spectrum from a two-layer source.

SUMMARY

A method for computing spectra from electronic transitions of diatomic and monatomic species has been described. The program has application for theoretical studies and analysis of experimental spectra as well. Examples describing its usefulness and versatility have been discussed.

Acknowledgements – The authors wish to thank Mrs. R. WINKLER for her help in running the computer program during its checkout and early production usage and Mr. H. WOODWARD for supplying part of the "*Q*-branch" data used in Fig. 2 and Table 3.

REFERENCES

1. E. E. WHITING, J. O. ARNOLD and G. C. LYLE, *JQSRT* **7**, 725 (1967).
2. E. E. WHITING, J. O. ARNOLD and G. C. LYLE, NASA TN D-5088 (1969).
3. W. G. VINCENTI and C. H. KRUGER, JR., *Introduction to Physical Gas Dynamics*, John Wiley, New York (1965).
4. S. S. PENNER, *Quantitative Molecular Spectroscopy and Gas Emissivities*, Addison-Wesley, Reading, Mass. (1959).
5. W. L. WIESE, M. W. SMITH and B. M. GLENNON, *Atomic Transition Probabilities. Volume I. Hydrogen Through Neon*, National Standard Reference Data Series, NBS-4 (1966).

6. G. HERZBERG, *Molecular Spectra and Molecular Structure. I. Spectra of Diatomic Molecules*, 2nd edn., Van Nostrand, New York (1950).
7. R. W. NICHOLLS and A. L. STEWART, Allowed Transitions. *Atomic and Molecular Processes* (Ed. D. R. BATES), Academic Press, New York (1962).
8. L. H. ALLER, *The Atmospheres of the Sun and Stars*, 2nd edn., The Ronald Press, New York (1963).
9. W. J. BORUCKI, NASA SP-3041 (1968).
10. A. SCHADEE, *JQSRT* **7**, 169 (1967).
11. E. V. STUPOCHENKO, I. P. STAKHANOV, E. V. SAMUILOV, A. S. PLESHANOV and I. B. ROZHDESTVENSKII, Thermodynamic Properties of Air Between 1000 and 12.000°K and 0.001 and 1000 Atmospheres. *Physical Gas Dynamics*, (Ed. A. S. PREDVODITELEV), Pergamon Press, Oxford (1961).
12. K. S. DRELLISHAK, *Partition Functions and Thermodynamic Properties of High Temperature Gases*, AEDC-TDR-64-22 (1964).
13. R. C. JOHNSON, *An Introduction to Molecular Spectra*, Methuen, London (1949).
14. L. T. EARLS, *Phys. Rev.* **48**, 423 (1935).
15. E. E. WHITING, *JQSRT* **8**, 1379 (1968).
16. L. WALLACE, *Astrophys. J.* **VII**, *Suppl.* 68, 165 (1962).
17. J. G. PHILLIPS and S. P. DAVIS, *The Red System ($A^2\Pi - X^2\Sigma$) of the CN Molecule*, University of California Press, Berkeley and Los Angeles (1963).
18. G. POLETTO and M. RIGUTTI, *Nuovo Cimento* **39**, 519 (1965).
19. H. T. WOODWARD, NASA TN D-3850 (1967).
20. R. J. SPINDLER, *JQSRT* **5**, 165 (1965).
21. A. E. DOUGLAS and P. M. ROUTLY, *Astrophys. J., Suppl.* **1**, 295 (1954).
22. E. A. BALLIK and D. A. RAMSAY, *Astrophys. J.* **137**, 84 (1963).
23. G. W. F. DRAKE, D. C. TYTE and R. W. NICHOLLS, *JQSRT* **7**, 639 (1967).
24. A. R. FAIRBAIRN, *JQSRT* **6**, 787 (1966).
25. R. W. NICHOLLS, *JQSRT* **2**, 433 (1962).

SYMBOLS

A_{ul}	Einstein A coefficient for spontaneous emission, sec^{-1}-part^{-1}
a	line-width parameter, dimensionless, $a = w_{l_N}/(ln\ 2/w_g)$
B_e	rotational constant in the equilibrium position, cm^{-1}
B_v	rotational constant for the vibrational level v, cm^{-1}, $[B_v = B_e - \alpha_e(v+\frac{1}{2})]$
B_λ	black-body emission, W(cm^2-μ-sr)$^{-1}$
C	integer in equation (20) that specifies whether lines with even or odd K'' are strongest in the spectra of homonuclear molecules
c	speed of light, $2{\cdot}9979 \times 10^{10}$ cm-sec^{-1}
D_e	rotational constant in the equilibrium position, cm^{-1}
D_v	rotational constant for the vibrational level v, cm^{-1}, $[D_v = D_e + \beta_e(v+\frac{1}{2})]$
d	electronic multiplicity, dimensionless
E	total integrated intensity due to spontaneous emission, W(cm^3-sr)$^{-1}$
$E_{v'v''}$	integrated intensity from (v', v'') band due to spontaneous emission, W(cm^3-sr)$^{-1}$
E_λ	spectral emission due to spontaneous emission, W(cm^3-μ-sr)$^{-1}$
e	electronic charge, $4{\cdot}80298 \times 10^{-10}$ esu (dyne-cm^2)
ea_0	product of electronic charge and radius of first Bohr orbit, $2{\cdot}5416 \times 10^{-18}$ esu cm (dyne-cm^3)
$F(K)$	rotational term function for the vibrational level v, cm^{-1}
$f_{el}(\lambda)$	wavelength dependent electronic absorption f-number, dimensionless
$G(v)$	vibrational energy, cm^{-1}
h	Planck's constant, $6{\cdot}623 \times 10^{-27}$ erg sec

I_λ	specific intensity, W(cm^2-μ-sr)$^{-1}$
J	total rotational quantum number, dimensionless
K	rotational quantum number without spin, dimensionless
k	Boltzmann constant, $1{\cdot}38054 \times 10^{-16}$ erg °K^{-1}
l	physical depth of radiating layer, cm
m	atomic or molecular weight, g mole
m_e	mass of the electron, $9{\cdot}1091 \times 10^{-28}$ g
N	number density of molecules, particles/cc
P	rotational branch with $\Delta J = -1$
Q	partition function, dimensionless, or rotational branch with $\Delta J = 0$
$q_{v'v''}$	Franck–Condon factor, dimensionless
R	rotational branch with $\Delta J = +1$
$\bar{r}_{v'v''}$	r-centroid or characteristic internuclear separation for the (v', v'') transition
$\Sigma\lvert R_e(\bar{r}_{v'v''})\rvert^2$	sum of the squares of the electronic transition moments, (esu cm)^2. The summation is over all electronic transitions between the upper and lower multiplet levels. (Note: More concise but less accurate descriptive phrases are used throughout the text)
S	quantum number of the resultant spin, dimensionless
$S^{J'\Lambda'}_{J''\Lambda''}$	line strength factor, dimensionless
T	temperature, °K (when T only is specified the case is in equilibrium and $T_{\text{elect}} = T_{\text{vib}} = T_{\text{rot}}$)
T_e	term energy of electronic state measured at the equilibrium position, cm^{-1}
T_{elect}, T_{vib}, T_{rot}	electronic, vibrational, and rotational temperatures, °K
v	vibrational quantum number, dimensionless
w_g	Gaussian line width at half-height, Å ($w_g = 7{\cdot}16 \times 10^{-7}\lambda\sqrt{T/m}$ for Doppler broadening)
w_l	Lorentzian line width at half-height, Å
w_v	Voigt line width at half-height, Å
α_e	rotational constant, cm^{-1}
α_λ	absorption coefficient, cm^{-1}
β_e	rotational constant, cm^{-1}
Λ	resultant orbital angular momentum of electrons along the internuclear axis, dimensionless
λ	wavelength, Å
λ_{CL}	line central wavelength, Å
$\Delta\lambda$	interval between points where spectral intensity is computed, Å
μ	wavelength, micron
ν	frequency of emitted radiation, sec^{-1}
$\bar{\nu}_{0(v'v'')}$	spectral location of band origin, cm^{-1}
ρ_0	density of air at 1 atm and 273°K, $1{\cdot}293 \times 10^{-3}$ g/cm^3
ρ/ρ_0	density, dimensionless
ω_e	vibrational constant, cm^{-1}
$\omega_e x_e$	vibrational constant, cm^{-1}
$\omega_e y_e$	vibrational constant, cm^{-1}
$\omega_e z_e$	vibrational constant, cm^{-1}

$( )'$	upper state, or indicates incident specific intensity or absorption coefficient corrected for induced emission
$( )''$	lower state
$( )_u$	upper state
$( )_l$	lower state